We are IntechOpen, the world's leading publisher of Open Access books
Built by scientists, for scientists

4,800
Open access books available

122,000
International authors and editors

135M
Downloads

Our authors are among the

154
Countries delivered to

TOP 1%
most cited scientists

12.2%
Contributors from top 500 universities

CLARIVATE ANALYTICS
BOOK CITATION INDEX
INDEXED

WEB OF SCIENCE™

Selection of our books indexed in the Book Citation Index in Web of Science™ Core Collection (BKCI)

Interested in publishing with us?
Contact book.department@intechopen.com

Numbers displayed above are based on latest data collected.
For more information visit www.intechopen.com

7

Nonlinear Bubble Behavior due to Heat Transfer

Ho-Young Kwak
Mechanical Engineering Department,
Chung-Ang University
Korea

1. Introduction

Previous studies of the forced oscillation of a spherical bubble in solution have been investigated by using the Rayleigh equation to obtain the time dependent bubble radius and a polytropic relation to obtain the gas pressure inside the bubble depending bubble volume (Lauterborn, 1976). In fact, the polytropic approximation with proper index values has been widely used for the gas undergoing quasi-equilibrium process in which there is heat transfer. However, the polytropic pressure-volume relationship fails to account the thermal damping due to heat transfer through the bubble wall because $P_b\, dV_b$ is a perfect differential and consequently its integral over a cycle vanishes (Prosperiretti et al., 1988) where P_b is the gas pressure inside the bubble and V_b is the bubble volume. Furthermore, the polytropic approximation assumes the uniform temperature for the gas intrinsically, which is valid only for a particular case and it is hard to tell whether the gas inside the bubble oscillating under ultrasound behaves isothermally or adiabatically (Loefstedt et al., 1993).

In this study, we have formulated a general bubble dynamics model, which is as follows. The density, velocity and pressure distributions for the gas inside a spherical bubble were obtained by solving the continuity and momentum equations analytically (Kwak et al., 1995, Kwak and Yang, 1995). With the set of analytical solutions for the conservation equations, the temperature distribution for the gas inside the bubble was also obtained by solving the energy equation for the gas. The heat transfer through the bubble wall was considered to obtain the instantaneous thermal boundary layer thickness from the mass and energy conservations for the liquid layer adjacent to the bubble wall by the integral method. The mass and momentum equations for the liquid outside the bubble wall provided the well known equation of motion for the bubble wall, the Rayleigh-Plesset equation in an incompressible limit or the Keller-Miksis equation in a compressible limit. The bubble dynamics model was applied to an evolving bubble formed form the fully evaporated droplet at the superheat limit (Kwak et al., 1995) and phenomena of sonoluminescence which is light emission associated with the catastrophic collapse of a micro-bubble oscillation under ultrasound (Young, 2005).

With uniform density, temperature and pressure approximations which are valid for the characteristic time scale of ms, the calculated values of the far field pressure signal from the evolving the bubble formed form the fully evaporated droplet at its superheat limit (Kwak et al., 1995) are in good agreement with the experimental results (Shepherd and Sturetevant, 1982). With uniform pressure approximation which is valid for the characteristic time scale

of μs, the calculated values of the minimum velocity of the bubble wall, the peak temperature and pressure are excellent agreement with the observed ones for the sonoluminescing xenon bubble in sulfuric acid solutions (Kim et al., 2006). Furthermore, the calculated bubble radius-time curve displays alternating pattern of bubble motion which is apparently due to the heat transfer for the sonoluminescing xenon bubble, as observed in experiment (Hopkins et al., 2005). The bubble dynamics model presented in this study has also revealed that the sonoluminescence for an air bubble in water solution occurs due to the increase and subsequent decrease in the bubble wall acceleration which induces pressure non-uniformity for the gas inside the bubble during ns range near the collapse point (Kwak and Na, 1996). The calculated sonoluminescence pulse width from the instantaneous gas temperature for air bubble is in good agreement with the observed value of 150 *ps* (Byun et al., 2005). Due to enormous heat transfer the gas temperature inside the sonoluminescing air bubble at the collapse point is about 20000~40000 K instead of 10^7 K (Moss et al., 1994) which is estimated to be in the adiabatic case. Molecular dynamics (MD) simulation results for the sonoluminescing xenon bubble were compared to the theoretical predictions and observed results (Kim et al., 2007, Kim et al., 2008).

2. Temperature profile in thermal boundary layer

A sketch of the bubble model employed is given in Fig.1, which shows a spherical bubble in liquid temperature T_∞ and liquid pressure P_∞. Heat transfer is assumed to occur through the thermal boundary layer of thickness δ(t). The temperature profile in this layer is assumed to be quadratic (Theofanous et al., 1969).

$$\frac{T - T_\infty}{T_{bl} - T_\infty} = (1 - \xi)^2 \tag{1}$$

where T_{bl} is the temperature at the bubble wall and T_∞ is the ambient temperature in Eq.(1). The parameter ξ in Eq.(1) is given as ξ = (r - R_b)/δ and $R_b(t)$ is the instantaneous bubble radius. Such a second order curve satisfies the following boundary conditions:

$$T(R_b, t) = T_{bl}, \quad T(R_b + \delta,\ t) = T_\infty \quad \text{and} \quad \left(\frac{\partial T}{\partial r}\right)_{r=R_b+\delta} = 0 \tag{2}$$

The heat transfer conducted through this thermal boundary layer whose thickness is δ(t) can be obtained by applying the Fourier law at the bubble wall, or

$$\dot{Q}_b = k_l A_b \left(\frac{\partial T}{\partial r}\right)_{r=R_b} = - \frac{8\pi R_b^2 k_l (T_{bl} - T_\infty)}{\delta} \tag{3}$$

where A_b is the surface area of bubble and k_1 is the conductivity of liquid. The bubble model including such liquid phase zone has been verified experimentally (Suslick et al., 1986).

3. Conservation equations for the gas inside bubble

The hydrodynamics related to studying the bubble behavior in liquid involves solving the Navier-Stokes equations for the gas inside the bubble and the liquid adjacent the bubble

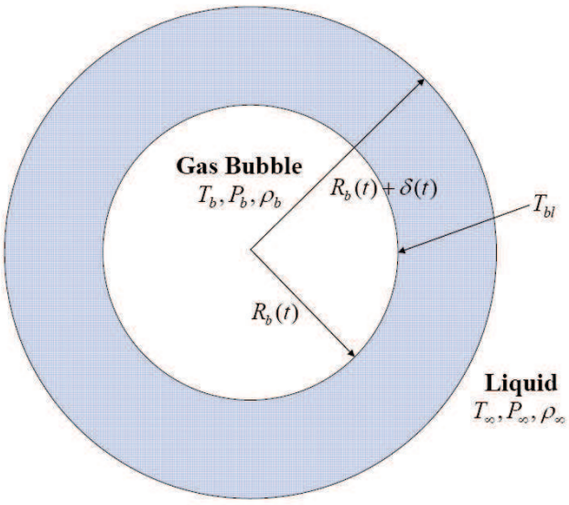

Fig. 1. A physical model with thermal boundary layer for a spherical bubble in liquid.

wall. Especially the knowledge of the behavior of gas or vapor inside evolving bubble is a key element to understand the bubble dynamics. Firstly, various conservation laws for the gas are considered to obtain the density, pressure and temperature distributions for the gas inside the bubble.

3.1 Mass conservation

The mass conservation equation for the gas inside a bubble is given by

$$\frac{D\rho_g}{Dt} + \rho_g \nabla \cdot \vec{u}_g = 0 \tag{4}$$

where ρ_g and u_g are gas density and velocity, respectively. With decomposition of the gas density in spherical symmetry as $\rho_0(t) + \rho_r(r,t)$, the continuity equation becomes

$$\left[\frac{d\rho_o}{dt} + \rho_o \nabla \cdot \vec{u}_g\right] + \frac{D\rho_r}{Dt} + \rho_r \nabla \cdot \vec{u}_g = 0 \tag{5}$$

where ρ_0 is the gas density at the bubble center and ρ_r is the radial dependent gas density inside the bubble and the notation of the total derivative used here is $D/Dt = \partial/t + u(\partial/\partial r)$. The rate of change of the density of a material particle can be represented by the rate of volume expansion of that particle in the limit $V \rightarrow 0$ (Panton, 1996). Or

$$u_g = \frac{\dot{R}_b}{R_b} r \tag{6}$$

With this velocity profile, the density profile can be obtained as

$$\rho_g = \rho_o + \rho_r \tag{7-1}$$

$$\rho_0 R_b^3 = \text{const.} \tag{7-2}$$

$$\rho_r = ar^2 / R_b^5 . \tag{7-3}$$

The constant, a is related to the gas mass inside a bubble (Kwak and Yang, 1995).

3.2 Momentum conservation

The momentum equation for the gas when neglecting viscous forces may be written as

$$\rho_g \frac{D\vec{u}_g}{Dt} = -\nabla P_b \tag{8}$$

The gas pressure P_b inside bubble can be obtained from this equation by using the velocity and density profiles given in Eq. (6) and (7), respectively. Or

$$P_b = P_{b0} - \frac{1}{2}\left(\rho_0 + \frac{1}{2}\rho_r \right)\frac{\ddot{R}_b}{R_b} r^2 \tag{9}$$

Note that the linear velocity profile showing the spatial inhomogeneities inside the bubble is a crucial ansatze for the homologous motion of a spherical object, which is interestingly encountered in another energy focusing mechanism of gravitational collapse (Jun and Kwak, 2000). The quadratic pressure profile given in Eq. (9), was verified recently by comparison with direct numerical simulations (Lin et al., 2002).

3.3 Energy conservation

Assuming that the internal energy for the gas inside a bubble is a function of gas temperature only as $de = C_{v,b}dT_b$, the energy equation for the gas inside the bubble may be written as

$$\rho_g \frac{De}{Dt} = \rho_g C_{v,b} \frac{DT_b}{Dt} = -P_b \nabla \cdot \vec{u}_g - \nabla \cdot \vec{q} \tag{10-1}$$

where Cv,b is the constant-volume specific heat and q is heat flux. The viscous dissipation term in the internal energy equation also vanishes because of the linear velocity profile. Since the solutions given in Eqs. (6), (7) and (9) also satisfy the kinetic energy equation, only the internal energy equation given in Eq. (10-1) needs to be solved. On the other hand, Prosperetti et al.(1988) solved the internal energy equation combined with the mass and momentum equation numerically to consider heat transport inside the bubble using a simple assumption. However, heat transfer through the liquid layer, which is very important in obtaining the temperature at the bubble wall, was not considered in their study.

Using the definition of enthalpy, the internal energy equation for the gas can also be written as

$$\rho_g \frac{Dh}{Dt} = \rho_g C_{p,b} \frac{DT_b}{Dt} = \frac{DP_b}{Dt} - \nabla \cdot \vec{q} \tag{10-2}$$

where $C_{p,b}$ is the constant-pressure specific heat. Eliminating DT_b/Dt from Eqs. (10-1) and (10-2), one can obtain the following heat flow rate equation for the gas pressure inside the bubble (Kwak et al., 1995, Kwak and Yang, 1995)

$$\frac{DP_b}{Dt} = -\gamma P_b \nabla \cdot \vec{u}_g - (\gamma - 1)\nabla \cdot \vec{q} \tag{11}$$

Rewriting Eq. (11), we have

$$(\gamma - 1)\nabla \cdot \vec{q} = -\frac{1}{R_b^{3\gamma}} \frac{D}{Dt}(P_b R_b^{3\gamma}) \tag{12}$$

which implies that the relation $P_b V^{3\gamma}$= const. holds if $\nabla \cdot q = 0$ inside the bubble.
Substituting Eq. (12) into Eq. (10), and rearranging the equation, we have

$$\frac{D}{Dt}\left\{\ln\left(\frac{P_b R_b^3}{T_b}\right)\right\} = \left(\frac{\rho_g R_g}{P_b} - \frac{1}{T_b}\right)\frac{DT_b}{Dt} \tag{13}$$

where R_g is gas constant. If the equation of state for ideal gas, $P_{bo} = \rho_g R_g T_{bo}$ holds at the bubble center, LHS in Eq. (13) vanishes. The result can be written as

$$P_{bo} R_b^3 / T_{bo} = const., \tag{14}$$

which is consistent with Eq.(7-2).
Note that the time rate change of the pressure at the bubble center can be written as with help of Eqs. (3) and (11).

$$\frac{dP_{bo}}{dt} = -\frac{3\gamma P_{bo}}{R_b}\frac{dR_b}{dt} - \frac{6(\gamma - 1)k_l(T_{bl} - T_\infty)}{\delta R_b} \tag{15}$$

The time rate change of the temperature at the bubble center can be obtained with help of Eq. (14). That is

$$\frac{dT_{bo}}{dt} = -\frac{3(\gamma - 1)T_{bo}}{R_b}\frac{dR_b}{dt} - \frac{6(\gamma - 1)k_l(T_{bl} - T_\infty)}{\delta R_b P_{bo}} \tag{16}$$

4. Temperature profiles inside the bubble

4.1 Uniform pressure profile inside the bubble

A temperature profile can be obtained by solving Eq. (12) with the Fourier law by assuming that the conductivity of gas inside the bubble is constant and the gas pressure inside the bubble is uniform (Kwak et al., 1995). That is

$$T_b = \frac{r^2}{6(\gamma - 1)k_g}\left[\frac{dP_b}{dt} + 3\gamma P_b \frac{\dot{R}_b}{R_b}\right] + T_{bo}(t) \tag{17}$$

where k_g heat conductivity of gas inside the bubble. The above equation can be written, with help of Eq.(12), as follows:

$$T_b = (T_{bo} - T_\infty)\left[1 - \left(\frac{r}{R_b}\right)^2 / (1 + \eta)\right] + T_\infty \tag{18}$$

where $\eta = \frac{k_g}{k_l}\frac{\delta}{R_b}$.

The temperature at the bubble wall can be obtained easily from the above equation. That is

$$T_{bl} = \left(T_\infty + \eta T_{bo}\right) / \left(1+\eta\right) \tag{19}$$

The above relation shows how the bubble wall temperature is related to the temperature at the bubble center and the ambient temperature. Assigning an arbitrary value on T_{bl} is not permitted as a boundary condition.

An uniform temperature distribution also occurs when there is no heat flux inside the bubble. This can be achieved when the bubble oscillating period is much longer than the characteristic time of heat diffusion so that the gas distribution function depends only on thermal velocity (thermal equilibrium case). In this limit, we may obtain the gas temperature inside the bubble by taking the value of the gas conductivity as infinity in Eq. (19). That is $T_b=T_{bl}=T_{bo}$, which validates the bubble dynamics formulation with an assumption of uniform vapor temperature inside the bubble (Kwak et al., 1995). The heat transfer through the thermal boundary layer adjacent to the bubble wall determines the heat exchange between the bubble and medium in this case.

However, the temperature gradient inside the bubble should exist, provided that characteristic time of bubble evolution is much shorter than the relaxation time of the vibration motion of the gases inside the bubble, which is of the order on 10^{-6}s for high gas temperature. If the temperature gradient inside the bubble exists inside the bubble, the heat transfer through the bubble wall depends on both the properties of the gas inside the bubble and the liquid in the thermal boundary layer. In this case one may rewrite Eq.(3), with help of Eq.(19). That is

$$\dot{Q}_b = -\frac{2A_b k_g (T_{bo} - T_\infty)}{R_b} / \left(1+\eta\right) \tag{20}$$

As long as the value of η is finite, there exists a temperature distribution inside the bubble. For a very small value of η, the heat flow rate from the bubble is solely determined from the temperature gradient of the gas inside the bubble (Prosperetti et al., 1988).

Assume the thermal conductivity for the gas inside the bubble is linearly dependent on the gas temperature such as

$$k_g = AT_b + B \tag{21}$$

For air $A=5.528\times10^{-5}$ W/mK^2 and $B=1.165\times10^{-2}$W/mK (Prosperetti et al., 1988) and for xenon, $A=1.031\times10^{-5}$ W/mK^2 and $B=3.916\times10^{-3}$ W/mK were used. With this approximation and Fourier law, one can obtain the following temperature profile by solving Eq. (12) with uniform pressure approximation, which is quite good until the acceleration and deceleration of the bubble wall is not significant. Thus

$$T_{\mathrm{b}}(r) = \frac{B}{A}\cdot\left[-1+\sqrt{(1+\frac{A}{B}T_{\mathrm{b}0})^2 - 2\frac{A}{B}(T_{\mathrm{bl}}-T_\infty)(\frac{r}{R_{\mathrm{b}}})^2 / \eta'}\right] \tag{22}$$

where $\frac{1}{\eta'} = \frac{B}{k_l}\frac{\delta}{R_b}$.

The temperature distribution is given in Eq. (22) is valid until the characteristic time of bubble evolution is of the order of the relaxation time for vibrational motion of the molecules (Vincenti and Kruger, 1965) and/or is much less than the relaxation time of the translational motion of the molecules (Batchelor, 1967). The temperature at the bubble wall T_{bl} can also be obtained with the thermal boundary conditions given in Eq.(2). That is

$$T_{bl} = -\frac{B}{A}\left(1+\frac{1}{\eta'}\right) + \frac{B}{A}\sqrt{\left(1+\frac{1}{\eta'}\right)^2 + 2\frac{A}{B}\left(T_{bo} + \frac{A}{2B}T_{bo}^2 + \frac{T_\infty}{\eta'}\right)} \tag{23}$$

For constant gas conductivity limit, or A→0 and B→ k_g the temperature distribution inside the bubble, Eq. (22), reduces to Eq. (18).

4.2 Non-uniform pressure profile

If the bubble wall acceleration has significant value, for example, the value exceed 10^{12} m/s^2, the second term is comparable to the first term in RHS of Eq.(9). This occurs for the sonoluminescing air bubble during few nanoseconds of collapse phase. Taking into account the bubble wall acceleration, the heat flow rate equation given in Eq. (12) may be rewritten as with help of Eqs. (6), (7) and (9)

$$(\gamma-1)\nabla\cdot\vec{q} = -\left[\frac{dP_b}{dt} + 3\gamma P_{bo}\frac{\dot{R}}{R_b}\right] + \frac{1}{2}\left(\rho_o+\rho_r\right)\left[(3\gamma-1)\frac{\dot{R}\ddot{R}}{R_b} + \frac{\dddot{R}}{R_b}\right]r^2 \tag{24}$$

Since the temperature rise due to the bubble wall acceleration is transient phenomenon occurred during few nanoseconds around the collapse point of the bubble, the above equation may be decomposed into

$$(\gamma-1)\nabla\cdot\vec{q}_o = -\left[\frac{dP_b}{dt} + 3\gamma P_{bo}\frac{\dot{R}}{R_b}\right] \tag{25-1}$$

and

$$(\gamma-1)\nabla\cdot(\vec{q}-\vec{q}_o) = \frac{1}{2}\left(\rho_o+\rho_r\right)\left[(3\gamma-1)\frac{\dot{R}\ddot{R}}{R_b} + \frac{\dddot{R}}{R_b}\right]r^2 \tag{25-2}$$

Abrupt temperature rise and subsequent rapid quenching due to the bubble wall acceleration and the increase and decrease in the acceleration may be treated in another time scale (Davidson, 1972), different from the bubble wall motion. A solution of Eq.(25-2) with no temperature gradient at the bubble center is given as

$$T_b'(r) = -\frac{1}{40(\gamma-1)k_g'}\left(\rho_o + \frac{5}{21}\rho_r\right)\left[(3\gamma-2)\frac{\dot{R}_b\ddot{R}_b}{R_b} + \frac{\dddot{R}_b}{R_b}\right]r^4 + C(t) \tag{26}$$

The coefficient C may be determined from a boundary condition $k_g dT_b/dr = k_l dT_l/dr$ at the wall where T_l is the temperature distribution in the thermal boundary layer with different

thickness δ'. Note that the boundary conditions employed for solving Eq. (25-1) and (25-2) are the same at the bubble center. However different properties of the gas was employed at the bubble wall so that the coefficient C(t) given in Eq. (26) is given as

$$C(t) = -\frac{1}{20(\gamma-1)}\left[(3\gamma-2)\dot{R}_b\ddot{R}_bR_b + \dddot{R}_bR_b^2\right]\left[\frac{\delta'}{k_l}\left(\rho_o + \frac{5}{14}\rho_{r=R_b}\right) + \frac{R_b}{2k_g'}\left(\rho_o + \frac{5}{21}\rho_{r=R_b}\right)\right] \quad (27)$$

The temperature distribution from Eq. (22) with low thermal conductivity k_g can be regarded as background one because the duration of the thermal spike represented by Eq. (26) is so short less than 500 ps. The gas conductivity at ultra high temperature k_g' may be obtained from collision integrals (Boulos et al., 1994). The value of δ' may be chosen so that proper bouncing motion results after the collapse and is about 0.1 μm. The final solution of the heat transport equation can be represented by the superposition of the temperature distributions caused by the uniform pressure and by the radial pressure variation induced by the rapid change of the bubble wall acceleration, as can be seen in equation (28); that is,

$$T(r) = T_b(r) + T_b'(r) \quad (28)$$

5. Navier-stokes equation for the liquid adjacent to the bubble wall

5.1 Bubble wall motion

The mass and momentum equation for the liquid adjacent bubble wall provides the well-known equation of motion for the bubble wall (Keller and Miksis, 1980), which is valid until the bubble wall velocity reaches the speed of sound of the liquid. That is

$$R_b\left(1-\frac{U_b}{C_b}\right)\frac{dU_b}{dt} + \frac{3}{2}U_b^2\left(1-\frac{U_b}{3C_b}\right) = \frac{1}{\rho_\infty}\left(1+\frac{U_b}{C_b}+\frac{R_b}{C_b}\frac{d}{dt}\right)\left[P_B - P_s\left(t+\frac{R_b}{C_b}\right) - P_\infty\right] \quad (29)$$

The liquid pressure on the external side of the bubble wall P_B is related to the pressure inside the bubble wall P_b according to:

$$P_B = P_b - \frac{2\sigma}{R_b} - 4\mu\frac{U_b}{R_b} \quad (30)$$

The driving pressure of the sound field P_s may be represented by a sinusoidal function such as

$$P_s = -P_A \sin\omega t \quad (31)$$

where $\omega = 2\pi f_d$.

The Keller-Miksis equation reduces to the well known Rayleigh equation which is valid at the incompressible limit without forcing field (Batchelor, 1967). That is

$$R_b\frac{dU_b}{dt} + \frac{3}{2}U_b^2 = \frac{1}{\rho_\infty}\left(P_B - P_\infty\right) \quad (32)$$

5.2 Thermal boundary layer thickness

The mass and energy equation for the liquid layer adjacent to the bubble wall with the temperature distribution given in Eq. (1) provides a time dependent first order equation for the thermal boundary layer thickness (Kwak et al., 1995, Kwak and Yang, 1995). It is given by

$$\left[1+\frac{\delta}{R_b}+\frac{3}{10}\left(\frac{\delta}{R_b}\right)^2\right]\frac{d\delta}{dt}=\frac{6\alpha}{\delta}-\left[2\frac{\delta}{R_b}+\frac{1}{2}\left(\frac{\delta}{R_b}\right)^2\right]\frac{dR_b}{dt} \\ -\delta\left[1+\frac{1}{2}\frac{\delta}{R_b}+\frac{1}{10}\left(\frac{\delta}{R_b}\right)^2\right]\frac{1}{T_{bl}-T_\infty}\frac{dT_{bl}}{dt} \tag{33}$$

The above equation which was discussed in detail by Kwak and Yang (1995) determines the heat flow rate through the bubble wall. The instantaneous bubble radius, bubble wall velocity and acceleration, and thermal boundary thickness obtained from Eqs. (29) and (33) provide the density, velocity, pressure and temperature profiles for the gas inside the bubble with no further assumptions. The gas temperature and pressure at the bubble center can be obtained from Eqs. (15) and (16), respectively.

The entropy generation rate in this kind of oscillating bubble-liquid system, which induces lost work for bubble motion needs to be calculated by allowing for the rate change of entropy for the gas inside the bubble and the net entropy flow out of the bubble as results of heat exchange (Bejan, 1988). That is

$$\dot{S}_g=\frac{DS_b}{Dt}-\frac{\dot{Q}_b}{T_\infty} \tag{34}$$

6. Calculated examples

6.1 An evolving bubble formed from the fully evaporated droplet at its superheat limit - Uniform temperature and pressure distributions for the vapor inside the bubble

It is well known that one may heat a liquid held at 1 atm to a temperature far above its boiling point without occurrence of boiling. The maximum temperature limit at which the liquid boils explosively is called the superheat limit of liquid (Blander and Katz, 1975). It has been verified experimentally that, when the temperature of a liquid droplet in an immiscible medium reaches its superheat limit at 1 atm, the droplet vaporizes explosively without volume expansion and the fully evaporated droplet becomes a bubble (Shepherd and Sturtevant, 1982). Since the internal pressure of the fully evaporated droplet is very large (Kwak and Panton, 1985, Kwak and Lee, 1991), the droplet expands spontaneously. At the initial stage of this process, the fully evaporated droplet expands linearly with time. However, its linear growing fashion slows down near the point where the nonlinear growing starts. The pressure inside the bubble may be taken as the vapor pressure given temperature with saturated vapor volume at the start of the nonlinear growing. Since the vapor pressure inside the bubble is still much greater than the ambient pressure, the bubble expands rapidly so that it overshoots the mechanical equilibrium condition and its size oscillates. In this case, since the temperature of the vapor inside the bubble is so low that

vibrational motion of the vapor is not excited and the characteristic time of bubble evolution of ms range is much longer than the relaxation time of the translational motion of vapor molecules, uniform temperature and pressure distribution for the vapor molecules inside the bubble are achieved (Kwak et al., 1995).

The calculated pressure wave signal from the evolving butane bubble in ethylene glycol at the ambient pressure of 1 atm and at a temperature of 378 K is shown in Fig. 2, together with the observed data (Shepherd and Sturtevant, 1982). In this case heat transfer occurs through the thermal boundary layer. Thermal damping due to finite heat transfer (Moody, 1984) is barely seen in this Figure. In Fig. 3(a), the time rate change of the vapor temperature during the bubble evolution is shown. As can be seen in this Figure,the bubble evolution is neither isothermal nor adiabatic. In Fig. 3(b), the entropy generation rate due to finite heat transfer for the evolving butane bubble is shown. As expected, the entropy generation during the bubble oscillation is always positive. More clear thermal damping can be observed from the far-field pressure signal of the evaporating droplet and evolving bubble formed from a cyclohexane droplet at its droplet, 492.0 K (Park et al., 2005) as shown in Fig.4. After first two volume oscillations, the original bubble has begun to disintegrate into a cloud of bubbles so that the far-field pressure signal becomes considerably smaller compared to the calculation results.

The far field pressure signal from the evolving bubble at a distance r_d from the bubble center can be written in terms of the volume acceleration of the bubble (Ross, 1976). Or

$$p(t) = \frac{\rho_\infty \ddot{V}_b}{4\pi r_d} = \frac{\rho_\infty}{r_d}(2R_b\dot{R}_b^2 + R_b^2\ddot{R}_b) \tag{35}$$

For the uniform temperature and pressure distribution, the bubble behavior can be calculated from Eqs. (15), (16), (19), (32) and (33) with appropriate initial conditions.

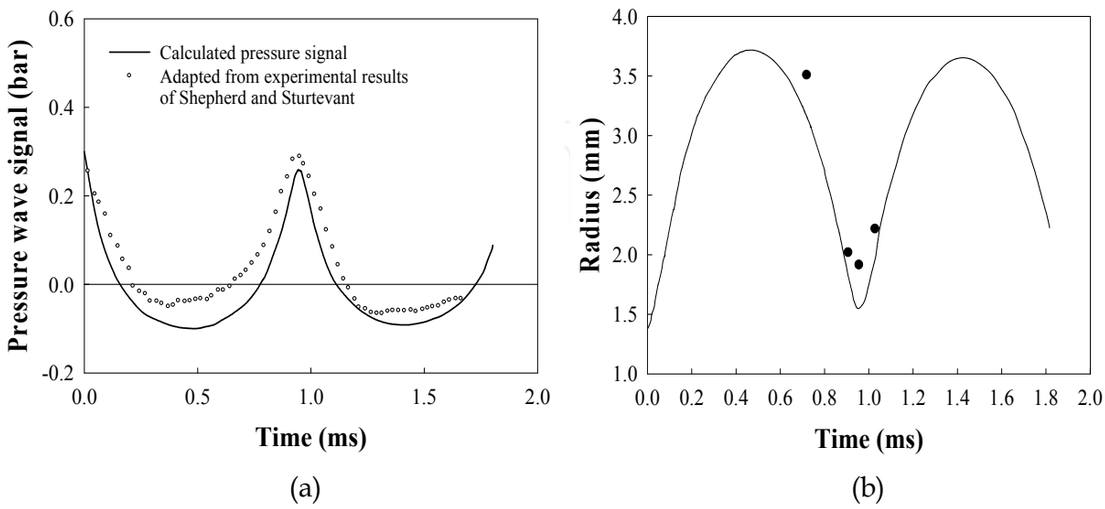

(a) (b)

Fig. 2. Pressure wave signal from a oscillating butane bubble in ethylene glycol at 1.013 bar (a) and radius-time curve for the butane bubble (b) with the observed results (full circles).

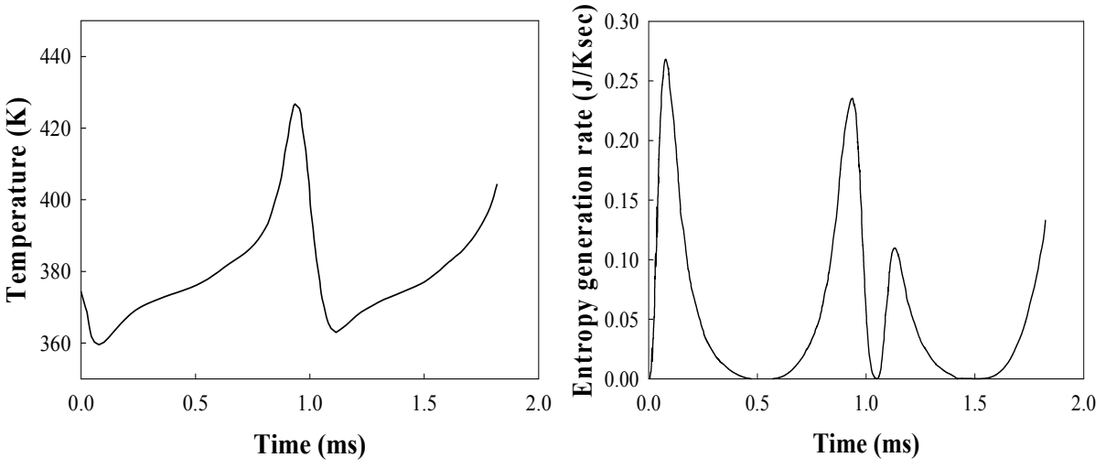

Fig. 3. Time dependence of the temperature inside the bubble (a) and time dependent entropy generation rate for the butane bubble (b) shown in Fig. 2.

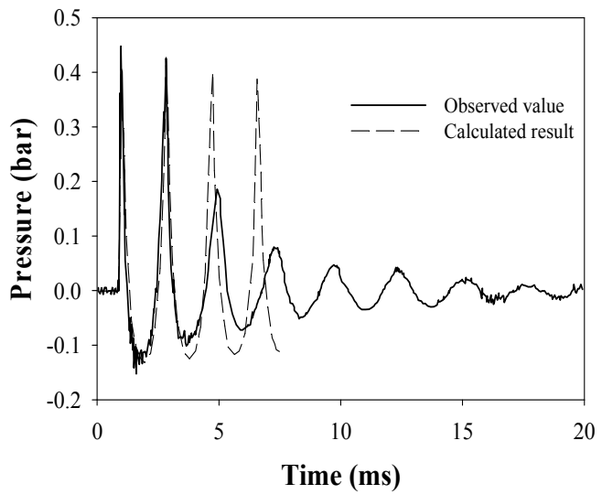

Fig. 4. Far-field pressure signal from an evolving bubble formed from a fully evaporated cyclohexane droplet at its superheat limit, 492.0 K in glycerine.

6.2 An air bubble oscillation under ultrasonic field---Non-uniform temperature and uniform pressure distribution for the gas inside bubble

If the gas temperature is above 2000 K, the vibrational modes of polyatomic molecules are expected to be excited. Since the relaxation time of the vibrational motion is rather long (10^{-6} s) compared with that of the translational motion, the perfect thermal equilibrium cannot be achieved for the duration in which mechanical equilibrium prevails. Certainly the temperature gradient for the gas inside bubble exists in this situation which is the case of an air bubble of micro size oscillates under ultrasonic field of amplitude below 1.2 atm and frequency of 26.5 kHz (Kwak and Yang, 1995).

The calculated radius–time curves for the bubble with an equilibrium radius of 8.5 μm , driven by the ultrasonic field with a frequency of 26.5 kHz and an amplitude of 1.075 atm which is certainly below the sonoluminescence threshold is shown in Fig.5. As shown in Table 1, the calculated values of the maximum radius and the period for each bouncing motion are in good agreement with the observed one (Loefstedt et al., 1993) can be seen. However, the bubble radius-time curve obtained by the Rayleigh equation with a polytropic relation of $P_bV_b^{1.4}$=const. shows 10 number of bouncing motions rather than 7.

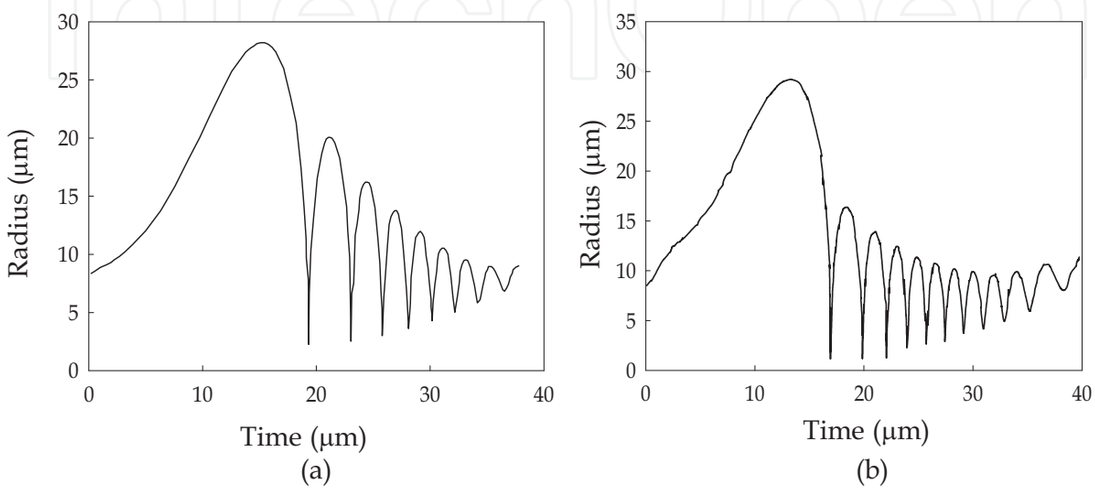

Fig. 5. Theoretical radius-time curves for an air bubble of R_o=8.5 μm at P_A=1.075 atm and f=26.5 kHz in water by our model (a) and by the Rayleigh-Plesset equation with polytropic relation (b).

Also the magnitude of the maximum bubble radius at the first bounce is significantly less than the observed one. The radius, the center temperature and pressure of the bubble at the collapse point are 2.23 μm, 2354 K and 518 atm, respectively (Kwak and Yang, 1995). The minimum bubble wall velocity at the bubble collapse point is about -111.5 m/s. In this case it is better to use Eq. (23) to obtain the bubble wall temperature and Eq. (29) to obtain the instantaneous bubble radius and velocity.

Bouncing number	Maximum bubble size (μm)		Corresponding period (μs)	
	Measured value	Calculated value	Measured value	Calculated value
1	19.9	20.0	3.56	3.62
2	15.6	16.2	2.43	2.76
3	13.0	13.6	2.24	2.24
4	11.1	12.1	2.06	2.07
5	10.4	10.5	1.87	1.90
6	9.7	9.5	1.87	1.82

Table. 1. Calculated and measured maximum bubble size and the corresponding period of bouncing motion after the first bubble collapse for air bubble of R_0 = 8.5 μm at P_A = 1.075 atm and f = 26.5 kHz.

6.3 Sonoluminescing xenon bubble in sulfuric acid solutions---Non-uniform temperature and almost uniform pressure distribution for the gas inside the bubble

Sonoluminecence (SL) phenomena associated with the catastrophic collapse of a gas bubble oscillation under ultrasonic field (Gaitan et al., 1992) have been studied extensively during last 20 years or so for their exotic energy focusing mechanism (Putterman and Weinger, 2000, Young, 2005). The SL from gas bubble in water is characterized by ten to hundred picoseconds flash (Gompf et al., 1997, Hiller et al., 1998), the bubble wall acceleration exceeding 10^{12} m/s^2 (Kwak and Na, 1996, Wininger et al., 1997), and submicron bubble radius at the collapse point (Weninger et al., 1997). On the other hand, the SL in sulfuric acid solution revealed rather longer flash widths of ns (Jeon et al., 2008), mild wall acceleration of 10^{10} m/s^2 (Hopkins et al., 2005) and micron bubble radius at the collapse point under similar conditions of ultrasonic field for the case of sonoluminescence in water.

The calculated radius-time curve along with observed results for a xenon bubble with R_o= 15 μm , driven by the ultrasonic field with a frequency of 37.8 kHz and an amplitude of 1.5 atm in aqueous solution of sulfuric acid is shown in Fig. 6. With air data for the thermal conductivity, the calculated radius-time curve which exactly mimics the alternating pattern of for the observed result shows two different states of bubble motion. With xenon data for the thermal conductivity, however, slight different pattern for the bubble motion was obtained. These calculation results imply that the bubble behavior, consequently the sonoluminescence phenomena depends crucially on the heat transfer in the gas medium as

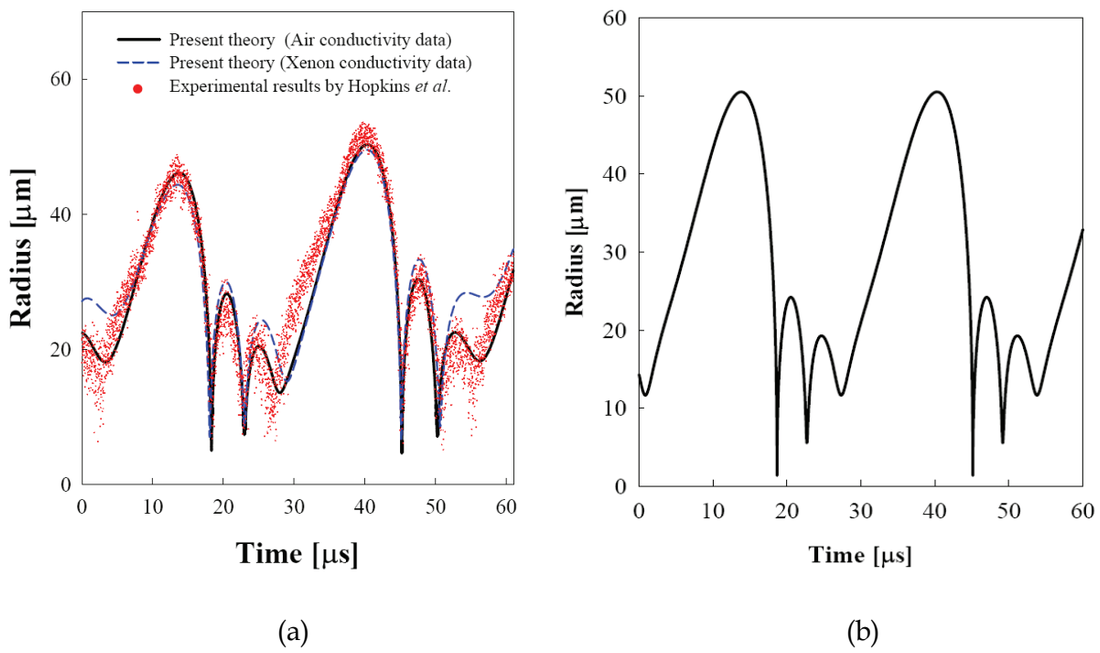

Fig. 6. Theoretical radius-time curve (a) along with observed one by Hopkins *et al.*(2005) for xenon bubble of R_0 =15.0 μm at P_A =1.50 atm and f_d =37.8 kHz in sulfuric acid solutions and the curve calculated by polytropic relation (b).

well as in the liquid layer and that the xenon bubble may contain a lot of air molecules. On the other hand the Rayleigh-Plesset equation with a polytropic relation, a conventional method used to predict the sonoluminescence phenomena cannot predict the two states of bubble motion as shown in Fig. 6(b). The alternating pattern for the bubble motion may happen due to the entropy generation by the finite heat transfer through the bubble wall, which produces lost work: less entropy generation in one cycle having lower maximum bubble radius provides more expansion work to the bubble next cycle, while larger amplitude motion experiencing more entropy generation provides less expansion work to the subsequent motion (Kim et al., 2006).

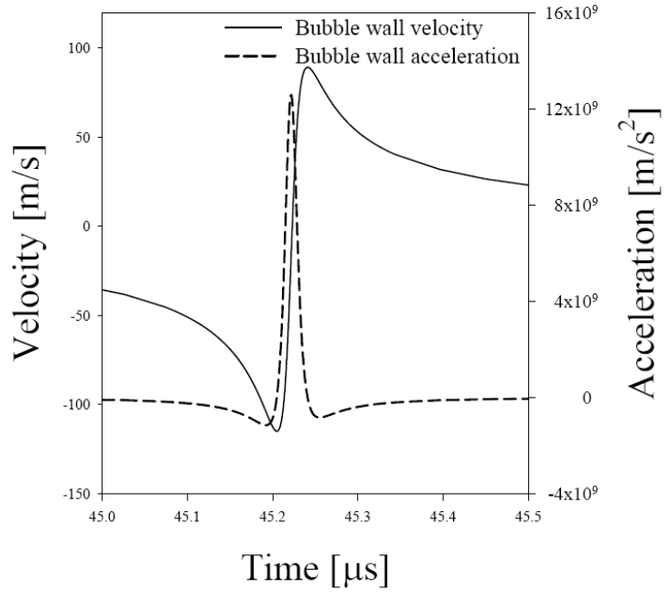

Fig. 7. Calculated bubble wall velocity (line) and acceleration (dash) near the collapse point for the bubble shown in Fig. 6.

Figure 7 shows the time-dependent bubble wall velocity and the variation of the bubble wall acceleration around the collapse point for the bubble shown in Fig. 6. The calculated magnitude of the minimum velocity at the collapse point for the light emitting cycles is about 115 m/s which is close to the observed velocity of 80 m/s. Whereas the maximum bubble wall velocity for non-light-emitting cycle is about 88 m/s, which is also close to the observed results of 60 m/s (Hopkins et al., 2005). However, the magnitude of the minimum velocity calculated by the Rayleigh-Plesset equation with the polytropic relation, which is about 900 m/s, is much higher than the observed value.

Figure 8 shows the calculated time-dependent bubble center temperature and the temporal emissive power with the average temperature for the light-emitting cycle of the bubble shown in Fig.6. The peak temperature calculated at the bubble center is about 8200 K, which is excellent agreement with the observed value of 6000~7000 K. In fact, the average temperature at the collapse point is about 6000 K because considerable temperature drop occurs at the bubble wall as shown in the insert. However, the pressure inside the bubble is almost uniform as expected as shown in Fig. 8 (b).

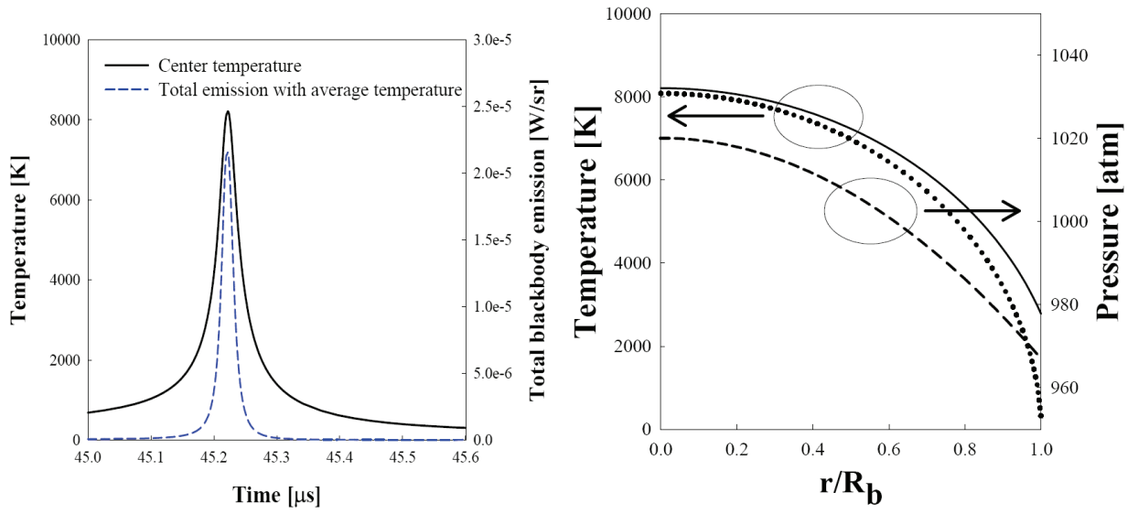

Fig. 8. Time dependent gas temperature at the bubble center and the corresponding total blackbody emission (a) with the average temperature and the temperature and pressure distributions at the collapse point for the bubble shown in Fig.6. The dotted curve in (b) indicates the temperature distribution obtained by Prosperetti eat al.'s (1988) boundary condition at the bubble wall.

6.4 Sonoluminescing air bubbles in water---Non-uniform temperature and non-uniform pressure distribution for the gas inside the bubble

When the bubble wall acceleration exceeds 10^{12} m/s^2, the pressure distribution for the gas inside the bubble is no longer uniform, as clearly confirmed by Eq. (9). In fact, the SL was observed for an air bubble in water or in sulfuric acid solution when the bubble wall acceleration exceeds 10^{12} m/s^2 ((Kim et al., 2006).

Figure 9 shows the density, pressure and temperature distributions inside the bubble at 400 ps before the collapse. Certainly, uniform pressure approximation is no longer valid during the collapsing phase for a sonoluminescing air bubble in water solution. Time dependent bubble wall acceleration and the gas temperature at the bubble center are shown in Fig. 10. As can be seen in this Figure, sudden increase and subsequent decrease in acceleration of the bubble wall results in rapid quenching of the gas followed by the substantial temperature rise up to 25000 K, which can be regarded as a thermal spike. Considerable increase in the gas temperature due to the bubble wall acceleration can be seen clearly in this Figure. The maximum bubble wall acceleration achieved near the bubble collapse point is over 10^{11} g (Kwak and Na, 1996), which is consistent with the observed value (Weininger et al., 1997). With uniform pressure approximation, the maximum temperature achieved is only 5800 K. On the other hand, the temperature of the gas inside the bubble goes to infinity without heat loss to the environment, that is k_g goes to zero. One may obtain the maximum temperature up to 10^7 K if one uses k_g= 0.01 W/mK, which indicates that heat transfer is very important also in this case. The heat flux at the collapse point is as much as 10 GW/m^2, however, the heat flow rate is about 2 mW.

The intense local heating and high pressure inside bubble and liquid adjacent to the bubble wall from such collapse that it can give arise to unusual effects in chemical reactions (Suslick, 1990), and the sonochemical process has been proven to be useful technique in making specialty nanomaterials (Kim et al., 2009). Note that the estimated temperature and pressure in the liquid zone around the collapsing bubble is about 1300 K and 1000 atm, respectively (Kwak and Yang, 1995).

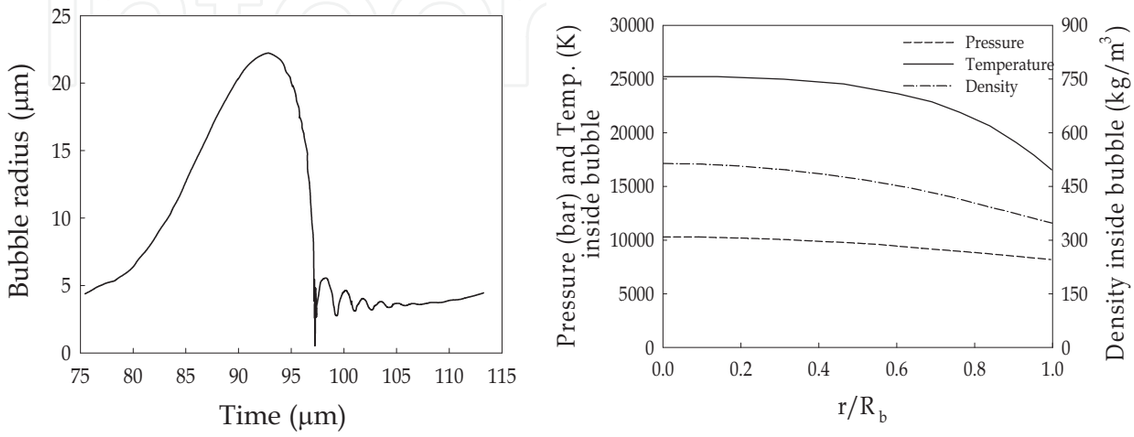

(a) (b)

Fig. 9. Theoretical radius-time curve for an air bubble of R_0 =4.5 μm at P_A =1.30 atm and f_d =26.5 kHz in water (a) and density , pressure and temperature distributions inside this bubble at 400 ps prior to the collapse point.

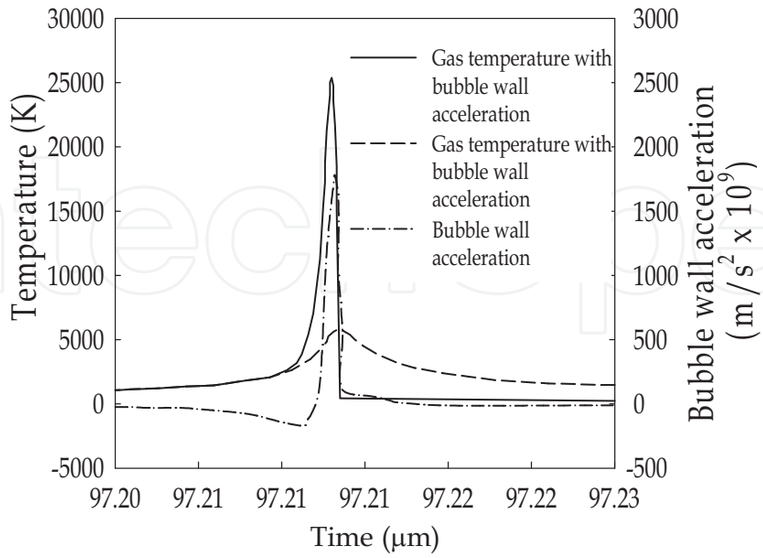

Fig. 10. Time dependent bubble wall acceleration and gas temperature around the collapse point for the case shown in Fig. 9.

7. Molecular dynamics simulation for sonoluminescing xenon bubble

In previous sections, the gas temperature inside the bubble depends crucially on the thermal conductivity of gas inside the bubble as well as the thermal conductivity of liquids in the thermal boundary layer. However, transport property values for the gas and liquid at the extreme condition are not available. As a consequence of this fact, validation of theoretical results was attempted through the MD simulation. The bubble radius was determined by the pressure obtained from MD simulation using Keller-Miksis equation. The mass transfer through the bubble wall, which does not affect the thermal properties at the collapse point very much (Kim and Kwak, 2007) was not considered in this simulation.

7.1 Molecular dynamics simulation

The principles and procedures for molecular dynamics simulation are well documented in standard text books (Haile, 1992, Rapaport, 1995). In this study, numerical integration of one million hard spheres was done in order to count the impulsive collisions between molecules moving by Newton's second law. As is well known, the kinetic events driven by Newton's law can be described by the Vlasov equation or the collisionless Boltzmann equation (Krall and Trivelpiece, 1973), which also yields the conservation equations for mass, momentum, and internal energy. This fact implies that MD simulation of hard sphere molecules might capture the physics related to SL phenomena. Furthermore, the soft parts of the potential are not significant for high energy collisions which occur near the collapse point (Ruuth et al., 2002).

7.2 Collision between molecule and bubble wall

The molecules inside the bubble may hit the molecules at the layer of the gas-liquid interface. In this simulation, the interface was assumed to be a hard wall, so that when a molecule hits the bubble wall, it reflects from the wall, as shown in Fig. 11. When considering the velocity of the bubble wall and assigning the thermal energy of the temperature at the bubble wall T_{bl}, the velocity of the reflected molecules $\vec{\mathbf{v}}_f$ may be obtained by the following equation for the heat bath boundary condition. In this case, the direction of the reflected particle may be assigned randomly or specularly (Kim et al., 2007).

$$\left|\vec{\mathbf{v}}_f - U_b\hat{\mathbf{r}}_i\right|^2 / 2 = (3/2)(k_B T_{bl} / m) \tag{36}$$

where U_b is the instantaneous bubble wall velocity, m is the mass of a molecule and k_B is the Boltzmann constant.

For the adiabatic boundary condition, the particles were assumed to be reflected from the wall with speed equal to the pre-collision speed in the local rest frame of the wall. The direction of reflected particles was determined according to the reflection law at the planar interface in this case. Explicitly, the velocity of the reflected particles is given by

$$(\vec{\mathbf{v}}_f - U_b\hat{\mathbf{r}}_i) = (\vec{\mathbf{v}}_i - U_b\hat{\mathbf{r}}_i) - 2\left[(\vec{\mathbf{v}}_i - U_b\hat{\mathbf{r}}_i)\cdot\hat{\mathbf{r}}_i\right]\hat{\mathbf{r}}_i \tag{37}$$

However, it has been found that neither the adiabatic nor the heat bath boundary condition is appropriate for treating the collapsing process of sonoluminescing gas bubbles. The heat

bath boundary condition means that heat flow exists at the bubble wall while adiabatic means no heat flow at the boundary. The degree of the adiabatic change during the collapsing process can be described by the following effective accomodation coefficient (Yamamoto et al., 2006):

$$\alpha = (T_{in} - T_{out}) / (T_{in} - T_{bl}) . \tag{38}$$

where T_{in} is the temperature of the gas particle moving toward the bubble wall and T_{out} is the temperature of particle leaving the wall. Two limiting cases are α = 0 for adiabatic boundary condition and α = 1 for the heat bath boundary condition.
For the adiabatic boundary case, a molecule does not lost its kinetic energy after a collision made with a molecule at the bubble wall. On the other hand, for the heat bath boundary case, a molecule having kinetic energy of T_i lost its kinetic energy to become a molecule having kinetic energy of T_{bl} after collision. The value of α defined in Eq. (38) determines the instantaneous gas temperature and pressure as well as the bubble radius and wall velocity via the heat transfer through the bubble wall.

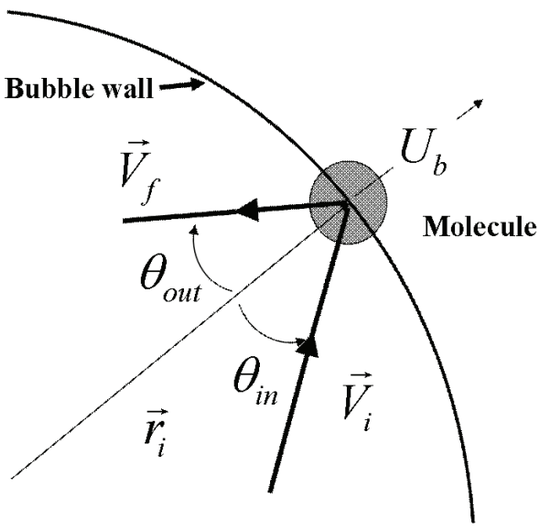

Fig. 11. A collision model between molecules and the bubble wall where v_i and v_f denote the velocity if incident and reflected molecule, respectively.

7.3 Calculation procedures

In this study, a sonoluminescing gas bubble in sulfuric acid solution was considered. The number of molecules in the sonoluminescing bubble may be obtained from the equation of state for an ideal gas.

$$P_\infty \left(\frac{4\pi}{3} {R_0}^3 \right) = N k_B T_\infty \tag{39}$$

where N is the number of molecules inside the bubble and P_∞ and T_∞ are the ambient pressure and temperature, respectively. For a sonoluminescing xenon bubble with an equilibrium radius of 0.7 μm in water at T_∞=300 K and P_∞=1 atm, the number of molecules occupying the bubble is about 3.5×10^7, which is difficult to handle with today's computing power.

One may use a scaling transformation for the molecular volume such as $V_g N = const.$ where V_g is the volume of gas molecule and N is the number of molecules occupying the bubble and that reduces the number of molecules that are handled in the MD simulation (Metten and Lauterborn, 2000). With this scaling transformation, of course, the mass and the energy of the system should be conserved so that $mN = const.$ and $TN = const.$

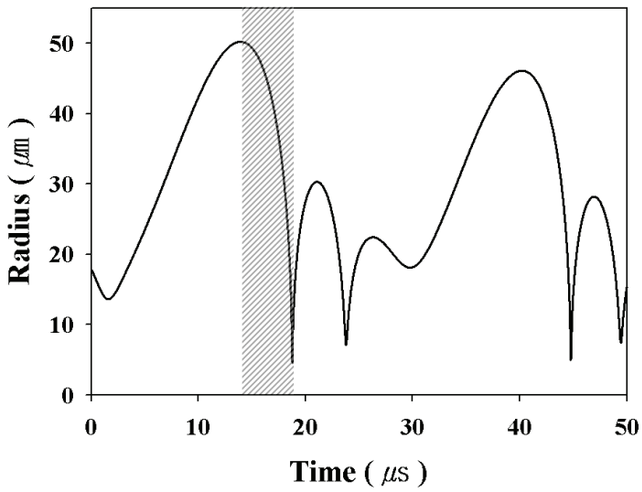

Fig. 12. Theoretical radius-time curves for a xenon bubble of R_o = 15 μm at P_A = 1.5 atm and f_d = 37.8 kHz in a sulfuric acid solution. Shaded area indicates the time span for MD simulations.

In this study, we chose number of simulated molecules to be 10^6, so the hard sphere diameter of a molecule increases to 71.79 σ for the xenon bubble of 15 μm in radius, where σ is the hard sphere diameter of the xenon molecule, taken to be 0.492 nm . The number 71.79 can be obtained from a relation $\sigma^3 N = \sigma_s^3 N_s$ with the number of simulated molecules of $N_s = 10^6$ and the total number of xenon molecules inside the bubble of equilibrium radius of 15 μm, $N = 3.46 \times 10^{11}$. The conversion factors for the bubble radius, pressure and temperature, which were used in this MD simulation are σ, ε/σ^3 and ε/k_B, respectively.

7.4 Calculation results and discussion

MD simulation for a collapsing xenon bubble with equilibrium radius of 15.0 μm, driven by an ultrasound frequency of 37.8 kHz and amplitude of 1.5 atm in sulfuric acid solution, was started at its maximum radius of 50.3 μm**.** The xenon bubble was chosen in this study because observed data for the bubble wall velocity and the peak pressure and temperature at the collapse point have been reported (Hopkins et al., 2005), which is same as the case shown in Fig. 6. One to three million particles were used for a scaled-down MD simulation of the bubble that actually had 35 million molecules. The initial gas state with temperature of 297.8 K and pressure of 3.64×10^{-2} atm was obtained from theoretical results obtained using a set of solutions of the Navier-Stokes equations for the gas inside the bubble with consideration of heat transfer through the bubble wall (Kwak and Yang, 1995, Kwak and Na, 1996). The cross-hatched region in Fig.12 indicates the time period of MD simulation for the xenon bubble which shows an on/off luminescence pattern in sulfuric acid solution (Hopkins et al., 2005).

In Fig.13, the bubble radius-time curve(a) and the time-dependent bubble wall velocity (b) near the collapse point, calculated by MD simulations with α =0.15 are plotted along with the theoretical results. The time-dependent gas temperature at the bubble wall, used in the MD simulation for employing the heat bath boundary condition, was calculated by theory. A very similar trend between MD simulation and theoretical calculation in the bubble radius-time curve and the time-dependent bubble wall velocity were obtained. It is noted that the theoretical minimum velocity at the collapse point, which is about -115 m/s, is close to the observed value of -80 m/s (Hopkins et al., 2005). The calculated value of the minimum velocity by MD is about -130 m/s. The best agreement between the MD simulation and the theoretical results was obtained with a value of α =0.15 among the trial of α values, 0.1, 0.15, 0.3 and 0.5. The minimum radius of the at the collapse point for the xenon bubble is about 4.56 μm so that the packing fraction at the point is about 0.058.

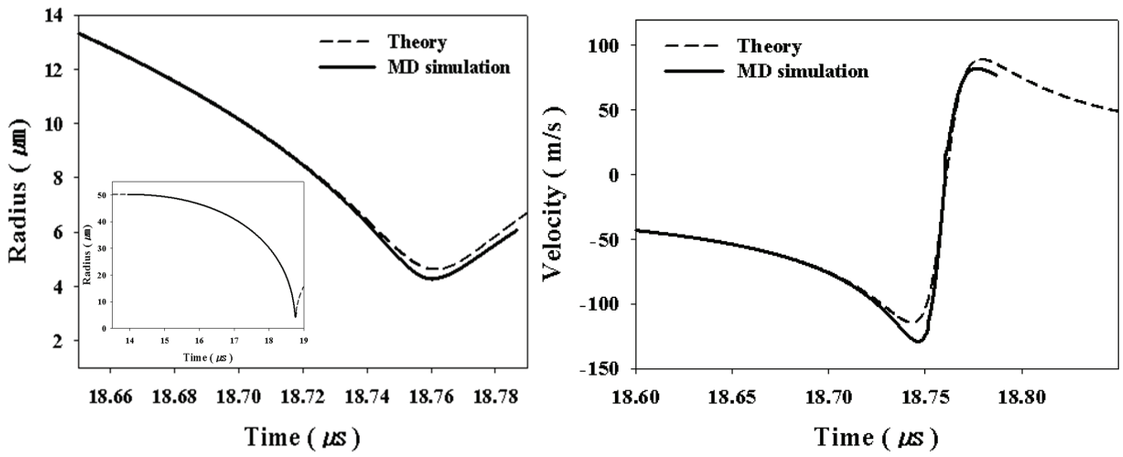

Fig. 13. Calculated radius–time curves (a) and time-dependent bubble wall velocity (b) obtained by MD simulation with α =0.15 and theory for the bubble shown in Fig. 12.

The time-dependent gas temperature and pressure inside the bubble around the collapse point, which were obtained by MD simulation with α =0.15 are shown in Fig.14. The peak temperature and pressure estimated by MD simulation are about 7,500 K and 1,260 atm, respectively, and are very close to the theoretically predicted values of 8,200 K and 1,010 atm, respectively. The MD simulation results shown in Figs.13 and 14 indicate that the collapsing process of a sonoluminescing micron bubble undergoes an almost adiabatic change although a large amount of heat transfer through the bubble wall occurs. At the moment of collapse, the heat flux at the bubble wall is much as 0.6 GW/m^2. A quite different collapsing process was obtained from the MD simulation with the heat bath boundary condition (α =1.0) (Kim et al., 2007): the compression was started very slowly at first and the final stage occurs very rapidly so that the estimated full width at half maximum (FWHM) of the luminescence pulse is about 5 ns, which is quite less than the value of the theoretical estimate of 20 ns (Kim et al., 2006).

Once the time dependent temperature for the gas inside the bubble around the collapse point, the FWHM of the light pulse can be estimated from the temperature profile with assumption of mechanism of the light emission (Kwak and Na, 1996, 1997). In Fig.15, the

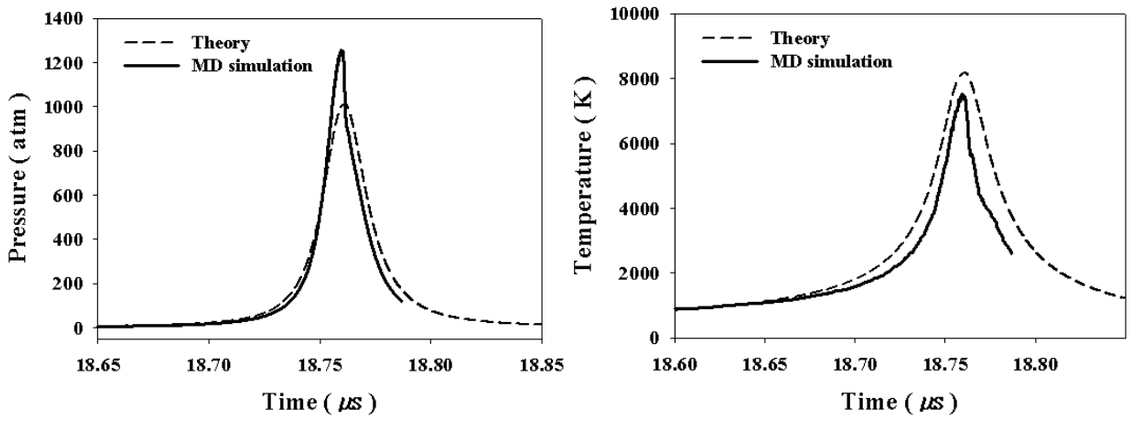

Fig. 14. Time-dependent center pressure (a) and temperature (b) obtained by MD simulation with α =0.15 and theory near the collapse point for the bubble shown in Fig. 12.

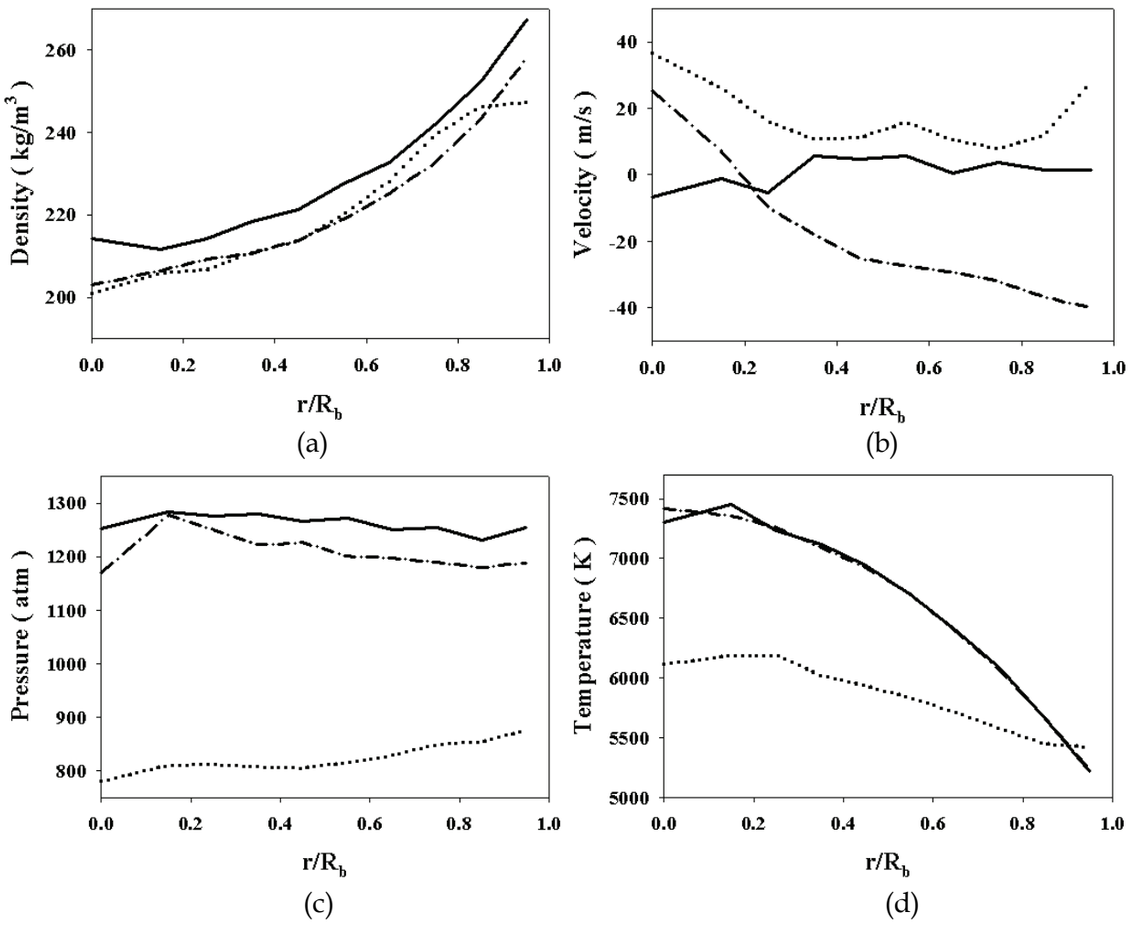

Fig. 15. Gas density(a), velocity(b), pressure(c), and temperature(d) distributions near the bubble collapse point obtained by MD simulation for the bubble shown in Fig.2 before 2.5 ns (— • — •), at (—) , and after 2.5 ns (• • • •) the collapse.

MD simulation results with α =0.15 for distribution of gas density(a), velocity(b), pressure(c), and temperature(d) are plotted before and at the collapse point for the bubble shown in Fig.12. The gas density increases radially in both compression and expansion phases, as predicted by theory. The magnitude of the gas velocity increases radially and has its maximum value at the bubble wall and a uniform null value at the collapse point, which can be predicted by the linear velocity profile obtained theoretically. The pressure has an almost uniform distribution before collapse. The temperature shows a quadratic profile with its minimum value near the bubble wall because of heat transfer, which can also be predicted by theory (Kwak and Yang, 1995, Kwak and Na, 1996, Kim et al., 2006).

8. Conclusions

A bubble dynamics model with consideration of heat transfer inside the bubble as well as in the thermal boundary layer of liquid adjacent to the bubble wall was discussed. Thermal damping due to finite heat transfer turns out to be very important factor for the evolving bubble formed from a fully evaporated droplet at its superheat limit and for the sonoluminescing xenon bubble showing two states of bubble motion in sulfuric acid solutions. Molecular dynamics simulation has been done to validate our theoretical model of bubble dynamics. In conclusion, the nonlinear behavior of an ultrasonically driven bubble and the sonoluminescence characteristics from the bubble in sulfuric acid solutions have been found to be correctly predicted by a set of solutions of the Navier-Stokes equations for the gas inside the bubble with considering heat transfer through the bubble wall.

9. References

Batchelor, G.K. (1967). *An Introduction to Fluid Dynamics*, Cambridge University Press, London.

Barber, B.P. & Putterman, S.J., Light scattering measurements of the repetitive supersonic implosion of a sonoluminescing bubble, *Phys. Rev. Lett*. Vol. 69, 3839, (1992).

Bejan, A. (1988). *Advanced Engineering Thermodynamics*, John Wiley & Sons, New York.

Blander , M. & Katz, J. L. (1975). Bubble nucleation in liquids, *AIChE J*. Vol. 21, No. 5, pp.833-848.

Boulos, M.I., Fauchais, P. & Pfender, E. (1994). *Thermal Plasma Vol.1* , Plenum Press, New York.

Byun,K., Kim, K.Y. & Kwak, H. (2005). Sonoluminescence characteristics from micron and submicron bubble, *J. Korean Phys. Soc.* Vol. 47, No. 6, pp.1010-1022.

Davidson, R.C. (1972). *Methods in Nonlinear Plasma Theory*, Academic Press, New York.

Gaitan, K.F., Crum, L.A., Church, C.C. & Roy, R.A.(1992). Sonoluminescence and bubble dynamics for a single, stable, cavitation bubble, *J. Acoust. Soc. Am*., Vol.91, pp.3166-3183.

Gompf, B., Guenter, R., Nick, G., Pecha, R. & Eisenmenger, W. (1997). Resolving sonoluminescence pulse width with time-correlated single photon counting, *Phys. Rev. Lett*., Vol. 79, pp. 1405-1407.

Haile , M. (1992). *Molecular Dynamics Simulation* ,John Wiley & Sons.

Hiller, R., Putterman, S.J. & Wininger, K.R. (1998). Time resolving spectra of sonoluminescence, *Phys. Rev. Lett*. Vol.80, pp. 1090-1093.

Hopkins, S.D., Putterman, S.J., Kappus, B.A., Suslick, K.S. & Camara, C.G. (2005). Dynamics of a sonoluminescing bubble in sulfuric acid, *Phys. Rev. Lett*. Vol.95, paper # 254301.

Jeon, J., Lim, C. & Kwak, H. (2008). Measurement of pulse width from sonoluminescing gas bubble in sulfuric acid solution, *J. Phys. Soc. Jpn*, Vol. 77, paper # 033703.

Jun, J. & Kwak, H. (2000). Gravitational collapse of Newtonian stars, *Int. J. Mod. Phys. D*, Vol.9, pp.35-42.

Keller, J.B. & Miksis, M. (1980). Bubble oscillations of large amplitude, *J. Acoust. Soc. Am*., Vol.68, pp.628-633.

Kim, H., Kang K. & Kwak, H. (2009). Preparation of supported Ni catalysts with a core/shell structure and their catalytic tests of partical oxidation of methane, *Int. J. Hydrogen Energy*, Vol. 34, pp. 3351-3359.

Kim, K., Byun, B. & Kwak, H. (2006). Characteristics of sonoluminescing bubbles in aqueous solutions of sulfuric acid, *J. Phys. Soc. Jpn*., Vol. 75, paper # 114705.

Kim, K. & Kwak, H. (2007). Predictions of bubble behavior in sulfuric acid solutions by a set of solutions of Navier-Stokes equations, Chem Eng. Sci., Vol. 62, pp. 2880-2889.

Kim, K., Kwak, H. & Kim, J.H. (2007). Molecular dynamics simulation of collapsing phase for a sonoluminescing gas bubble in sulfuric acid solutions : A comparative study with theoretical results, *J. Phys. Soc. Jpn.* Vol.76, 024301.

Kim, K.Y., Lim, C., Kwak, H. & Kim J.H. (2008). Validation of molecular dynamic simulation for a collapsing process of sonoluminescing gas bubble, *Mol. Phys*., Vol. 106, No. 8, pp. 967-975.

Krall, N.A. &Trivelpiece, A.W.(1973). P*rinciples of Plasma Physics* ,McGraw-Hill, New York.

Kwak, H. & Lee, S. (1991). Homogeneous bubble nucleation predicted by molecular interaction model, *ASME J. Heat Trans*. Vol. 113, pp. 714-721.

Kwak, H. & Na, J. (1996). Hydrodynamic solutions for a sonoluminescing gas bubble, *Phys. Rev. Lett*., Vol.77, pp.4454-4457.

Kwak, H. & Na, J. (1997). Physical processes for single bubble sonoluminescence, *J. Phys. Soc, Jap*. Vol.66, pp.3074-3083.

Kwak, H., Oh, S. & Park, C. (1995). Bubble dynamics on the evolving bubble formed from the droplet at the superheat limit, *Int. J. Heat Mass Transfer*, Vol.38, pp.1707-1718.

Kwak, H. & Panton, R.L. (1985). Tensile strength of simple liquids predicted by a model of molecular interactions, *J. Phys. D: Appl. Phys*., Vol. 18, pp.647-659.

Kwak, H. & Yang,H. (1995). An aspect of sonoluminescence from hydrodynamic theory, J. Phys. Soc. Jpn. Vol. 64, 1980-1992.

Lauterborn, W. (1976). Numerical investigation of nonlinear oscillation of gas bubbles in liquids, *J. Acoust. Soc. Am*., Vol. 99, pp. 283-293.

Lin, H., Storey, B.D. & Szeri, A.J.(2002). Inertially driven inhomogenieties in violently collapsing bubbles: the validity of the Rayleigh-Pessset equation, *J. Fluid Mech*., Vol.452, pp.145-162.

Loefstedt, R., Barber, B.P. & Putterman, S.J. (1993). Toward a hydrodynamic theory of sonoluminescence, *Phys. Fluids*, Vol. A5, pp. 2911-2928.

Metten, B. & Lauterborn, W. (2000). In Nonlinear Acoustics at the Turn of the Millennium: ISNA 15, 15th International Symposium on Nonlinear Acoustics edited by W. Lauterborn and T. Kurz, AIP Conf. Proc. No. 524, pp. 429-432.

Moody, F.J. (1984). Second law thinking-example application in reactor and containment technology, In *Second Law Aspects of Thermal Design* (Edited by A. Bejan and R.C. Reid) Vol. HTD-33, pp. 1-9. ASME, New York.

Moss,W.C., Clarke, D.B., White, J.W. & Young, D.A.(1994). Hydrodynamic simulations of bubble collapse and picosecond sonoluminescence, *Phys. Fluids*, Vol.6, No. 9, pp. 2979-2985.

Na, J., Byun, G. & Kwak, H. (2003) Diffusive stability for sonoluminescing gas bubble, *J. Kor. Phys. Soc*. Vol. 42,pp.143-152.

Panton, R.L. (1996). *Incompressible Flow*, John Wiley & Sons, 2nd Edition, New York.

Park, H., Byun, K. & Kwak, H. (2005). Explosive boiling of liquid droplets at their superheat limits, *Chem. Eng. Sci.*, Vol. 60, pp. 1809-1821.

Prosperetti, A., Crum, L. A. & Commander, K. W. (1988). Nonlinear bubble dynamics, *J. Acoust. Soc. Am.*, Vol.88, pp.1061-1077.

Putterman, S.J. & Weininger, K.R. (2000). Sonoluminescence: How bubbles turn sound into light. Annual Review of Fluid Mech., Vol. 32, pp. 445-476.

Rapaport,D.C.(1995). *The Art of Molecular Dynamics Simulation*, Cambridge University Press, London.

Ross, D. (1976). *Mechanics of Underwater Noise*, Pergamon Press, Oxford.

Ruuth, S.J., Putterman, S. & Merriman, B. (2002). Molecular dynamics simulation of the response of a gas to a spherical piston: Implications for sonoluminescence, *Phys. Rev. E*, Vol. 66, 036310.

Shepherd, J.E. & Sturtevant, B. (1982). Rapid evaporation at the superheat limit, *J. Fluid Mech.*, Vol. 121, pp. 379-402.

Suslick, K.S. (1990). Sonochemistry, Science, Vol. 247, pp. 1439-1445.

Suslick, K.S., Hammerton, D.A. & Cline, R.E. (1986). The sonochemical hot spot, *Am. Chem. Soc.*, Vol. 108, pp. 5641-5642.

Theofanous, T., Biasi, L. & Isbin, H.S.(1969). A theoretical study on bubble growth in constant and time-dependant pressure fields, *Chem. Eng. Sci.*, Vol.24, pp.885-897.

Vincenti, W.G. & Kruger, C.H. (1965). *Introduction to Physical Gas Dynamics*, New York.

Weninger, K.R., Barber, B.P. & Putterman, S.J. (1997). Pulsed Mie scattering measurements of the collapse of a sonoluminescing bubble, Phys. Rev. Lett., Vol. 78, pp. 1799-1802.

Yamamoto,K., Takeuchi,H. & Hyakutake, T. (2006). Characteristics of reflected gas molecules at a solid surface, *Phys. of Fuids*, Vol.18,046103.

Young, F.R.(2005). *Sonoluminescence* , CRC Press, Boca Raton.

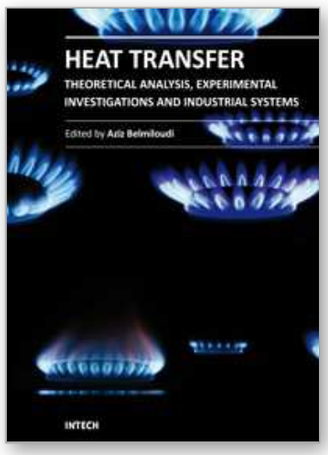

Heat Transfer - Theoretical Analysis, Experimental Investigations and Industrial Systems

Edited by Prof. Aziz Belmiloudi

ISBN 978-953-307-226-5
Hard cover, 654 pages
Publisher InTech
Published online 28, January, 2011
Published in print edition January, 2011

Over the past few decades there has been a prolific increase in research and development in area of heat transfer, heat exchangers and their associated technologies. This book is a collection of current research in the above mentioned areas and discusses experimental, theoretical and calculation approaches and industrial utilizations with modern ideas and methods to study heat transfer for single and multiphase systems. The topics considered include various basic concepts of heat transfer, the fundamental modes of heat transfer (namely conduction, convection and radiation), thermophysical properties, condensation, boiling, freezing, innovative experiments, measurement analysis, theoretical models and simulations, with many real-world problems and important modern applications. The book is divided in four sections : "Heat Transfer in Micro Systems", "Boiling, Freezing and Condensation Heat Transfer", "Heat Transfer and its Assessment", "Heat Transfer Calculations", and each section discusses a wide variety of techniques, methods and applications in accordance with the subjects. The combination of theoretical and experimental investigations with many important practical applications of current interest will make this book of interest to researchers, scientists, engineers and graduate students, who make use of experimental and theoretical investigations, assessment and enhancement techniques in this multidisciplinary field as well as to researchers in mathematical modelling, computer simulations and information sciences, who make use of experimental and theoretical investigations as a means of critical assessment of models and results derived from advanced numerical simulations and improvement of the developed models and numerical methods.

How to reference

In order to correctly reference this scholarly work, feel free to copy and paste the following:

Ho-Young Kwak (2011). Nonlinear Bubble Behavior due to Heat Transfer, Heat Transfer - Theoretical Analysis, Experimental Investigations and Industrial Systems, Prof. Aziz Belmiloudi (Ed.), ISBN: 978-953-307-226-5, InTech, Available from: http://www.intechopen.com/books/heat-transfer-theoretical-analysis-experimental-investigations-and-industrial-systems/nonlinear-bubble-behavior-due-to-heat-transfer

INTECH
open science | open minds

InTech Europe
University Campus STeP Ri
Slavka Krautzeka 83/A
51000 Rijeka, Croatia

InTech China
Unit 405, Office Block, Hotel Equatorial Shanghai
No.65, Yan An Road (West), Shanghai, 200040, China
中国上海市延安西路65号上海国际贵都大饭店办公楼405单元

Phone: +385 (51) 770 447
Fax: +385 (51) 686 166
www.intechopen.com

Phone: +86-21-62489820
Fax: +86-21-62489821

IntechOpen

IntechOpen

© 2011 The Author(s). Licensee IntechOpen. This chapter is distributed under the terms of the Creative Commons Attribution-NonCommercial-ShareAlike-3.0 License, which permits use, distribution and reproduction for non-commercial purposes, provided the original is properly cited and derivative works building on this content are distributed under the same license.

IntechOpen

IntechOpen